Published in Journal of Colloid and Interface Science 271 (2004) 163–173

Characterization of the pores in hydrous ferric oxide aggregates formed by freezing and thawing

Annette Hofmann,[a,*] Manuel Pelletier,[b] Laurent Michot,[b] Anna Stradner,[c] Peter Schurtenberger,[c] and Ruben Kretzschmar[a]

[a] *Institute of Terrestrial Ecology, Swiss Federal Institute of Technology (ETH) Zurich, Grabenstrasse 3, CH-8952 Schlieren, Switzerland*
[b] *Laboratoire Environnement et Minéralurgie, UMR INPL et CNRS N° 7569, Centre de Recherche François Fiessinger, 15 avenue du Charmois, F-54501 Vandoeuvre les Nancy, France*
[c] *Physics Department, Soft Condensed Matter Group, Université de Fribourg, Chemin du Musée 3, Perolles, CH-1700 Fribourg, Switzerland*

Received 26 March 2003; accepted 21 November 2003

Abstract

Hydrous ferric oxides (HFO) are efficient sorbents for inorganic and organic pollutants and therefore have great potentials in environmental science and engineering applications. Freezing and thawing of HFO suspensions leads to the formation of dense HFO aggregates. It facilitates the handling and increases the drying rate of HFO. In this study, we used a combination of pycnometry, gas adsorption (N_2 gas, water vapor), and small-angle neutron scattering (SANS) to characterize the porosity and pore size distribution of dense HFO aggregates formed by freezing dialyzed HFO suspensions at $-25\,^{\circ}C$ and thawing them at room temperature. The crystallinity of the HFO, which was a 2-line ferrihydrite, was not affected by this treatment. Wet sieving and laser diffraction analysis showed that the dense HFO aggregates had a unimodal size distribution with an average diameter of 235 ± 35 μm. Increasing the freezing rate by cooling with liquid N_2 ($-196\,^{\circ}C$) resulted in much smaller aggregates with an average diameter of 20 μm. Adding $NaNO_3$ electrolyte to the HFO suspensions prior to freezing also resulted in the formation of smaller aggregates. The dense HFO aggregates formed at $-25\,^{\circ}C$ had a porosity of $0.73 \pm 0.02\ l l^{-1}$. SANS revealed a unimodal size distribution of pores, with an average pore diameter of 2.0 nm. The diameter of the HFO crystallites was estimated by transmission electron microscopy to be 1.9 ± 0.5 nm. Geometrical considerations taking into account the unit particle and average pore size suggest that the crystallites retain 1–2 layers of hydration water during the coagulation induced by freezing. Analysis by N_2 gas adsorption showed that drying the dense HFO aggregates induced a reduction in porosity by about 25% and shifted the pore size distribution to smaller diameters. Rewetting during water vapor adsorption did not induce significant changes of the aggregate structure. The specific surface area of the dry HFO aggregates was between 320 and 380 $m^2\,g^{-1}$.

Keywords: Hydrous ferric oxide; Pore size; Micropores; Mesopores; Surface area; Aggregation; Freeze–thaw conditioning; Surface hydration; Density; Neutron scattering; Gas adsorption; Electron microscopy

1. Introduction

Hydrous ferric oxides (HFO) are poorly crystalline, highly porous solids with large specific surface areas, ranging from 200 to 750 $m^2\,g^{-1}$ ([1] and review therein). The mineral–water interface of HFO has a pH-dependent charge and is highly reactive with respect to chemisorption of protons, metal cations, oxyanions, and organic molecules [2]. In addition to adsorption reactions, precipitation of HFO can lead to incorporation of metal contaminants into the HFO structure by co-precipitation [3,4]. Because of its properties as an effective sorbent for numerous inorganic and organic pollutants in soils and water, HFO plays an important role in pollution abatement of contaminated soils, water treatment technology, and the metal and mining industries. For example, HFO can be effectively used to remove arsenate or phosphate from contaminated water [5,6].

The high water content of freshly precipitated HFO poses a serious problem for applications in water treatment, because it results in high drying and disposal costs. Thus,

* Corresponding author. UMR CNS 8110, Processus et Bilans des Domaines Sédimentaires, Université des Sciences et Technologies Lille 1, F-59655 Villeneuve d'Ascq Cedex, France.
E-mail address: annette.hofmann@univ-lille1.fr (A. Hofmann).

0021-9797
doi:10.1016/j.jcis.2003.11.053

methods for the dewatering of HFO suspensions are quite important. One technique, which has been known since at least the 19th century [7], is based on freezing and thawing. It leads to the formation of dense HFO aggregates and improves the filtration [8] and drying behavior [9] of HFO. A thorough investigation of the conditions of formation and some basic physical characteristics of freeze and thaw products of HFO and hydrous Mn oxide suspensions was undertaken by Vol'khin, Zolotavin, and co-workers in the early 1960s [8,10–13]. Using methods such as gravimetric particle size and density analysis and vacuum filtration, the researchers investigated the effect of freezing temperature, electrolyte type, and concentration on the formation of dense aggregates by freezing and thawing. Their findings show that the rate of nucleation of the ice and the cryohydrates governs the aggregate characteristics, in particular the aggregate size, the moisture content, and the filterability of a layer of sedimented aggregates. The higher the freezing rate, the smaller and the more compact were the resulting aggregates. Undertaking unidirectional freezing experiments, the authors inferred that cryosuction by diffusion of the water molecules to the ice surface is the main process responsible for the HFO compaction. Van der Giessen [14] used the freeze and thaw technique with liquid nitrogen as the refrigerant to produce fine HFO powder. Later studies investigated dense aggregates of various metal oxyhydroxides as a sorbent material for heavy metals and radionuclides [15]. Several attempts have been made to make the technique available in water treatment plants, notably for the reduction of alum sludges [9,16,17]. Driehaus et al. [18] proposed the use of HFO aggregates in fixed bed reactors for the purification of natural waters contaminated with arsenic. Dense HFO aggregates formed by freezing and thawing also occur naturally, for example, in soils of cold regions where freezing and thawing cycles shape the soil's porosity and aggregate structure [19,20].

The surface area and pore structure of HFO aggregates formed by freezing and thawing have not been previously investigated in detail. The objective of our study was to investigate the external and internal specific surface area, porosity, and pore structure of dense HFO aggregates formed by freezing and thawing. A detailed understanding of the pore structure of such aggregates is a prerequisite for interpreting and modeling the frequently observed slow sorption kinetics of cations and anions to HFO aggregates, which may be limited by pore diffusion [21–23].

2. Materials and methods

2.1. Synthesis of HFO aggregates

Hydrous ferric oxide (HFO) was synthesized following the procedure of Schwertmann and Cornell [24] by titrating a 0.2 M $Fe(NO_3)_3$ solution to pH 8 with 1 M KOH. The resulting precipitate, a two-line ferrihydrite, was allowed to settle and the supernatant solution was replaced by deionized water. After two repetitions of this washing procedure, the suspension was dialyzed (Spectra/Por, MWCO 12-14000) for 15 days against deionized water. The dialysis was performed at 4 °C to prevent transformation of the HFO to a more crystalline phase. After dialysis, the HFO was transferred to 1-liter glass bottles (Schott Duran) and mixed for about 10 min, until a homogeneous HFO suspension was obtained. It was diluted with deionized water to give an approximate HFO concentration of 2 $g\,l^{-1}$. The dilute suspension was transferred to 500-ml high-density polyethylene containers, shaken, and immediately frozen at −25 °C in a laboratory freezer. The initial freezing rate of the HFO suspensions was 2 $mm\,h^{-1}$ along the container walls and 5 $mm\,h^{-1}$ at the bottom, in contact with the ice-covered shelf. After one to several weeks, the frozen HFO was allowed to thaw at room temperature, which left the HFO aggregates formed during the freezing process intact. In the following, we will use the labels *fresh HFO* for the freshly prepared HFO suspension without freezing, and *dense HFO* for the large HFO aggregates formed by the freezing and thawing treatment, respectively.

Two dialyzed HFO samples were subjected to 10 subsequent freezing (−25 °C) and thawing (25 °C) cycles or 10 cooling (4 °C) and warming (25 °C) cycles, respectively. The main purpose was to observe possible effects of temperature changes or freezing on the crystallinity of the HFO aggregates.

The influence of the freezing rate on HFO aggregate formation was studied by comparing the size distributions of dense HFO aggregates formed by freezing at −25 °C and at −196 °C in liquid N_2 (approximately 1000 $mm\,h^{-1}$). Similarly, the effect of electrolyte concentration on aggregate formation was investigated by comparing the size distributions of HFO aggregates formed by freezing a dialyzed HFO suspension and HFO suspensions with 0.1 or 1.0 M $NaNO_3$ electrolyte concentration at −25 °C, respectively. The salt additions were made 1 h prior to freezing. For the temperature and salt dependency studies, small flasks with volume 50 ml were used instead of the 500-ml containers of the standard preparation procedure.

2.2. Morphology of HFO aggregates

The morphology of the fresh HFO and dense HFO aggregates was investigated by high-resolution scanning electron microscopy (HR-SEM) and transmission electron microscopy (TEM), respectively. Dilute HFO suspensions were air-dried onto carbon-coated collodion films supported by a 200 mesh TEM Cu grid. The samples were examined at a magnification of 800,000× on a Leo 9-12 Omega TEM. Sizing of HFO unit crystallites by TEM was performed with an estimated scaling error of ±5%. For HR-SEM, the samples were first evacuated to 10^{-8} bar and sputter-coated with a 1-nm monolayer of tungsten. The samples were then exam-

ined on a Hitachi S-900 SEM equipped with an in-lens field emission gun.

2.3. Crystallinity of HFO aggregates

The crystallinity of the fresh HFO and the dense HFO aggregates submitted to the different freezing and thawing and warming and cooling cycles was characterized by powder X-ray diffraction analysis (XRD). Subsamples of about 50 mg of all HFO suspensions were freeze-dried, gently ground in an agate mortar, and then pressed onto silicon sample holders previously coated with a thin layer of Vaseline. Diffraction patterns were recorded on a Bruker D8 θ–θ powder diffractometer using Cu$K\alpha$ radiation with a scintillation counter equipped with a secondary monochromator. All scans were recorded for Bragg angles of 15° to 70° 2θ with a step size of 0.03° 2θ and a scan rate of 0.0075° 2θ s^{-1}. Each sample was measured in triplicate and counts were added.

2.4. Size distribution of HFO aggregates

The size distribution of the dense HFO aggregates formed by the specific temperature and electrolyte freezing and thawing treatments was analyzed by laser diffraction (Malvern Mastersizer MS 20) using a 2-mW He–Ne laser emitting at wavelength 633 nm. For each measurement, the 100-ml liquid sample cell was filled with deionized water and thoroughly degassed and 100 to 200 mg of HFO particles were added. We used a 300-nm lens suitable for a particle size range of 1.2 to 600 μm. The particle size distributions were resolved into 32 bands.

For one selected sample of dialyzed HFO frozen at −25 °C, the size distribution measured by laser diffraction was independently verified by comparing it to a size distribution obtained by wet sieving. This analysis was performed in duplicate starting with 1 g of HFO per measurement. A suite of mesh sizes with 1000, 500, 315, 200, 100, and 50 μm cut-off diameter was used in cascade. Aggregate size separation was achieved by washing each sieve with a gentle jet of deionized water. All size fractions were dried at 40 °C and weighed.

2.5. Density of wet HFO aggregates

The density of the wet HFO aggregates formed by freezing at −25 °C and subsequent thawing was determined by pycnometry. Shortly after thawing, suspensions containing approximately 2 g of dense HFO aggregates were passed through 0.45-μm cellulose acetate membrane filters (Sartorius) using a low vacuum. Filtration was continued until the filter residue had a dry appearance, indicating that interaggregate water had been removed. The aggregates themselves retained their full moisture content in this procedure. Calibrated 20-ml pycnometer glass vials were filled with deionized water and temperature-equilibrated in a water bath set to 25 °C. To each pycnometer, a weighed quantity of 1.5 to 2 g of wet HFO aggregates was added. The volume of that amount of HFO was determined by weighing the total mass of the pycnometer before and after the HFO addition. The density of the wet HFO aggregates was obtained by the ratio of total mass to total volume. The density determination was performed in triplicate.

2.6. Surface area and porosity by gas adsorption

The specific surface area and the micro- and mesoporosity of the dense HFO aggregates formed by freezing at −25 °C and thawing was investigated by N_2 gas and water vapor adsorption and desorption experiments. For the N_2 gas adsorption/desorption isotherms, the samples were first outgassed at 30, 50, or 80 °C at 10^{-9} bar for a period of 18 h. For metastable minerals such as HFO, a low outgassing temperature is generally chosen to avoid recrystallization of the sample during measurement. However, Stanjek and Weidler [25] showed that dry heating of two-line ferrihydrite at moderate temperature (125 °C) did not induce recrystallization after 1150 h. The weight loss upon heating is attributed to loss of surface and structural OH groups, but without net changes in unit cell and XRD coherence lengths. Outgassing at 50 and 80 °C in this study serves to control the quality of data obtained at lower outgassing temperature. The measurements were conducted at liquid-N_2 temperature (−196 °C), with the samples kept in a bath of liquid N_2 at constant level. The N_2 gas pressure was established with a lab-built step-by-step volumetric setup. The purity of N_2 gas was >99.995%. Pressure measurements were carried out with two absolute gauges (Edwards) in the ranges 0–0.01 bar and 0–1 bar. The saturation pressure of nitrogen at −196 °C was recorded during the whole experiment using a third gauge. The adsorption isotherm was obtained from the measurement of equilibrium pressures before and after contact with the sample.

Water vapor adsorption and desorption measurements were carried out with a continuous gravimetric apparatus built around a Setaram MTB 10-8 symmetrical balance [26]. Prior to each experiment, the sample was outgassed under vacuum (10^{-9} bar) at a temperature of 30 °C. Water vapor was supplied from a liquid source kept at 45 °C, through a leak valve (Edwards), at a flow rate slow enough to ensure quasi-equilibrium conditions at all times. Pressures were measured with an absolute gauge (0–0.13 bar, Druck).

Both N_2 gas and water vapor adsorption isotherms were fitted with the Brunauer–Emmet–Teller (BET) equation to determine the specific surface area [27]. The *t*-plot method of assessing the microporosity of the HFO aggregates [28,29], was applied to the N_2 gas adsorption isotherms. The size distribution of pores in the range between pore diameters 2 and 95 nm (mesopores) was evaluated by applying the Barrett–Joyner–Halenda (BJH) method [30,31] to the N_2 gas desorption isotherm data. For the BJH calculations, the pore shape was assumed to be cylindrical.

2.7. Pore size distribution by neutron scattering

Small-angle neutron scattering (SANS) allows the determination of micro- and mesopores in a suspension. The pore size distribution of the fully hydrated HFO dense aggregates can be investigated by this method. We performed SANS experiments on the SANS1 instrument at the SINQ small-angle scattering facility of the Paul Scherrer Institut (PSI, Switzerland). Dense HFO aggregates formed by freezing a dialyzed HFO suspension at $-25\,^{\circ}$C and subsequently thawing it at room temperature were equilibrated in D_2O. For measurement the samples were kept in stoppered quartz cells (Hellma) with a path length of 2 mm and thermostated at 25 °C. The wavelength λ for all experiments was 0.8 nm with a wavelength resolution of 10% (full width at half maximum value). All measurements were done with a 30-cm detector offset. A q-range of 2.5×10^{-2} to 3 nm^{-1} was covered by three sets of sample-to-detector distances ($d = 1.6$, 6, and 18 m). The neutron spectra of water were measured in a 1-mm-path-length quartz cell. The raw spectra were corrected for background scattering due to the solvent (D_2O), the effect of the sample cell, and for electronic noise. Furthermore, the two-dimensional isotropic scattering spectra were corrected for detector efficiency by dividing by the incoherent scattering spectra of pure water and were azimuthally averaged. In the model fitting procedure the ideal scattering curve $I_{id}(q)$ was first calculated for a given pore size distribution. This $I_{id}(q)$ was then smeared with the instrumental resolution function and compared with the experimentally measured data. The pore size distribution was then optimized using the standard least-squares methods [32,33] and the errors were calculated by conventional methods [34].

3. Results

3.1. Morphology and crystallinity

The XRD patterns of fresh HFO and HFO aggregates produced by various freezing and thawing treatments are presented in Fig. 1. All diffractograms correspond to two-line ferrihydrite with only two broad diffraction peaks, indicating d-spacings of 0.250 and 0.148 nm, respectively. The various freezing/thawing or cooling/warming treatments induced slight sharpening of the 0.221 and 0.196 shoulders. Yet even after 10 freezing/thawing cycles the sample was still a pure two-line ferrihydrite. These results are in general agreement with earlier reports for HFO [14] and other hydroxides [35].

The morphology of the fresh HFO as observed by TEM is illustrated in Fig. 2a. One can clearly observe the unit crystallites of the HFO, which are estimated to be 1.9 ± 0.5 nm in diameter. This size is in good agreement with data published by Janney and co-workers [36] for a two-line HFO synthesized using a similar procedure. Fig. 2b shows a typical HR-SEM image of the fresh HFO after dialysis. Although

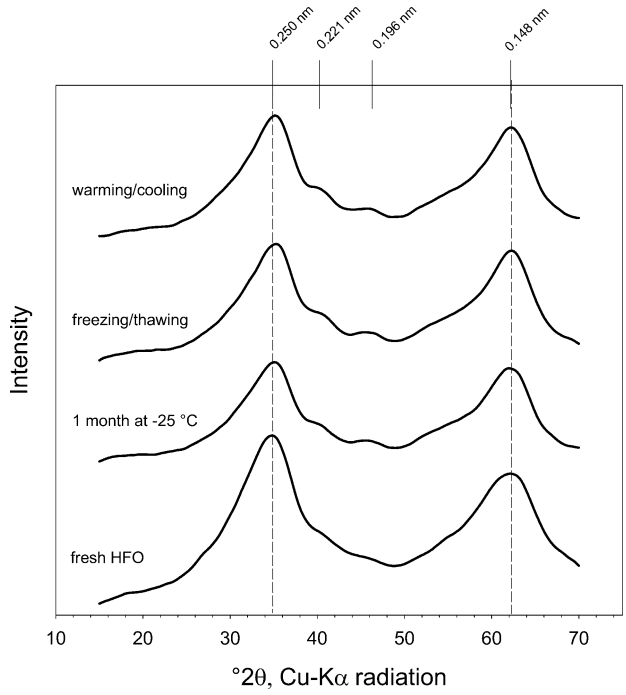

Fig. 1. Powder X-ray diffraction patterns of the fresh HFO, the dense HFO aggregates formed by freezing at $-25\,^{\circ}$C (and kept at this temperature for one month), the HFO subjected to 10 freezing/thawing cycles, and HFO subjected to 10 cooling/warming cycles.

some contraction of the aggregate structure may occur during drying and evacuation, the HFO aggregates appeared open-structured and branched, with large voids and irregular porosity. In contrast to this morphology, the dense HFO aggregates formed by freezing and thawing are much larger and consist of densely packed unit crystallites (Figs. 2c and 2d). The porosity appears to be reduced to minimum interstitial space (Fig. 2d). Some very large μm-sized cracks are observed at the surfaces of the dense aggregates (Fig. 2c); they may have formed during evacuation in the sputtering chamber.

3.2. Size distribution

The size distributions of dense HFO aggregates formed by freezing under various conditions and subsequent thawing at room temperature are depicted in Fig. 3. Fig. 3a shows the size distribution of the dense HFO aggregates formed by freezing a dialyzed HFO suspension at $-25\,^{\circ}$C. The size distribution determined by laser diffraction is unimodal with a volume mean of 235 μm and a standard deviation of the distributions of 130 μm. About 85% of all aggregates were smaller than 500 μm; 60% were between 100 and 300 μm in diameter. Reproducibility between different sample preparations is very good, with a variability of the mean size of 15%. The inset of Fig. 3a shows a comparison of the size distribution of the same sample obtained by laser diffraction (smooth line) and by wet sieving and gravimetric analysis (step line). The weighted average aggregate diameter ob-

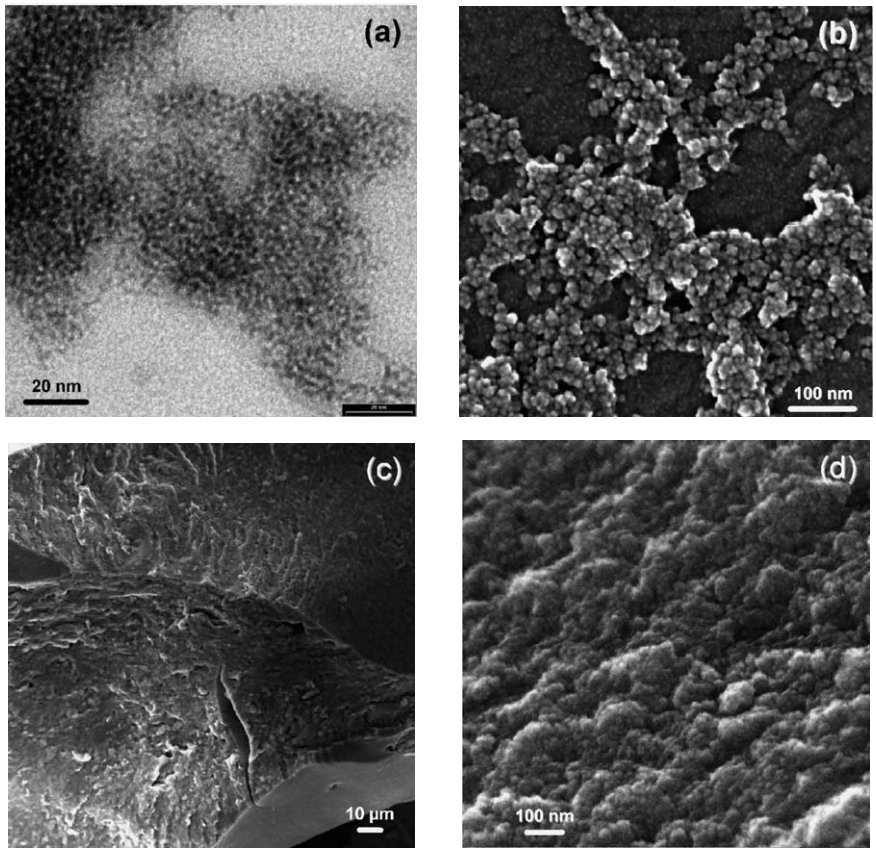

Fig. 2. Typical transmission and high-resolution scanning electron microscopy (TEM, HR-SEM) images of the fresh HFO and dense HFO aggregates: (a) TEM image of fresh HFO exhibiting unit crystallites with an average diameter of 1.9 ± 0.5 nm, (b) HR-SEM image of fresh HFO exhibiting an open aggregate structure, (c) HR-SEM image of a dense HFO aggregate formed by freezing at $-25\,^{\circ}$C, and (d) HR-SEM image of a dense HFO aggregate at higher magnification.

tained by wet sieving was 275 µm. The results obtained by the two methods are in good agreement. Therefore, the aggregate size distributions of all other samples were only determined by laser diffraction.

The influence of the freezing temperature, and thus the freezing rate, is demonstrated in Fig. 3b. At $-196\,^{\circ}$C the freezing rate was much higher than at $-25\,^{\circ}$C, and this resulted in the formation of much smaller HFO aggregates, which also exhibited an approximately lognormal size distribution but had an average diameter of 20 µm. The effect of electrolyte concentration on HFO aggregate formation is illustrated in Fig. 3c. With increasing electrolyte ($NaNO_3$) concentration, the average diameter of the HFO aggregates decreased. It was reduced to 90 µm in 0.1 M $NaNO_3$ and to 20 µm in 1 M $NaNO_3$, respectively.

As opposed to the dense HFO aggregates, fresh HFO aggregates do not have a definitive size that can be unambiguously determined by laser-diffraction. Because aggregates have a branched, open structure, the mechanical shear produced by mixing of the suspension induces reorganization of the aggregate structure, increasing the fractal dimension and decreasing their size [37]. Tentative measurements with ionic strengths of 1 and 10 mM showed average aggregate sizes of 70 and 40 µm at a pH of 7.5 and a 10-min mixing period.

3.3. Surface area and porosity

The dense HFO aggregates formed by freezing the dialyzed HFO suspension at $-25\,^{\circ}$C were investigated in detail for porosity, pore size distribution and surface area using pycnometry, gas adsorption techniques, and small-angle neutron scattering (SANS). The density of the wet HFO aggregates as determined by pycnometry was 1.81 ± 0.06 g cm^{-3}. This is less then 50% of the density of dry HFO (3.96 g cm^{-3} [38]) and corresponds to a total porosity of 0.73 ± 0.02 l l^{-1} (73%). Zolotavin and co-workers [8] obtained HFO aggregates with 66% porosity by freezing at $-15\,^{\circ}$C. Driehaus et al. [18] quote 75–80% porosity for HFO aggregates but without reporting the temperature used to freeze the suspension. Variations may be due to the efficiency with which interaggregate water was removed during filtration of the suspension before pycnometer analysis. The validity of the results presented here was cross-checked in flow-through experiments by independently determining the mobile pore volume of a column wet-packed with HFO aggregates. Similar results, that is, a density of 1.86 ± 0.12 g cm^{-3} or a porosity of 71 ± 4.6%, were obtained for the dense HFO aggregates. Differences from the literature data may also be due to the value chosen for the density of dry HFO, which depends on the degree of sur-

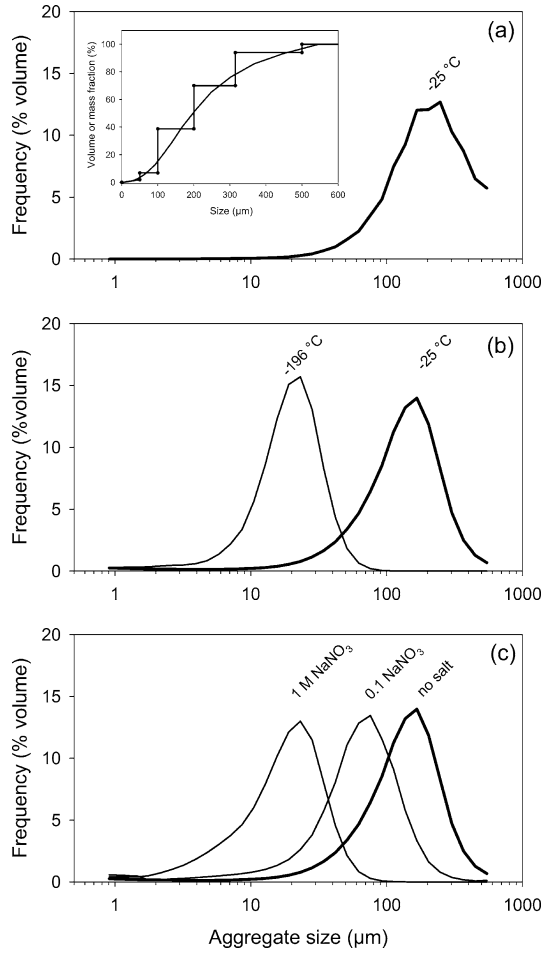

Fig. 3. Aggregate size distributions of dense HFO aggregates formed by freezing and thawing, as determined by laser diffraction analysis: (a) Dense HFO aggregates formed by freezing the dialyzed HFO suspension at $-25\,^{\circ}\mathrm{C}$ and thawing at room temperature. The inset shows the cumulative size distribution determined by laser diffraction (continuous curve) and wet sieving (step curve). (b) Dense HFO aggregates formed by freezing the dialyzed HFO suspension at -25 and $-196\,^{\circ}\mathrm{C}$. (c) Dense HFO aggregates formed by freezing a dialyzed HFO suspension and HFO in the presence of 0.1 and 1 M $NaNO_3$ electrolyte at $-25\,^{\circ}\mathrm{C}$. For the experiments (b) and (c) with different freezing temperatures and electrolyte concentrations, 100 mg HFO was frozen in 50-ml flasks, instead of 1 g in 500 ml as in experiment (a). Compared to (a) the curve of dialyzed HFO frozen at $-25\,^{\circ}\mathrm{C}$ in (b) and (c) is shifted to slightly smaller aggregate sizes. This shift is attributed to the change in freezing volume.

face hydration and is not easily determined. The value used in this work was determined by Towe and Bradley [38] in a crystallographic study and should be close to the dehydrated mineral density.

The pore size distribution of the HFO aggregates was investigated by a SANS experiment. Fig. 4a shows the neutron scattering intensity $I(q)$ of the HFO in D_2O as a function of the scattering vector q. Generally, $I(q) \sim P_{\mathrm{eff}}(q) S_{\mathrm{eff}}(q)$, where the so-called form factor $P_{\mathrm{eff}}(q)$ contains information about the size distribution, while the structure factor $S_{\mathrm{eff}}(q)$ reflects the spatial arrangement of the pores. In Fig. 4a we observe a steep power-law-like decrease at low q-values followed by a weaker decay at intermediate and high q-values.

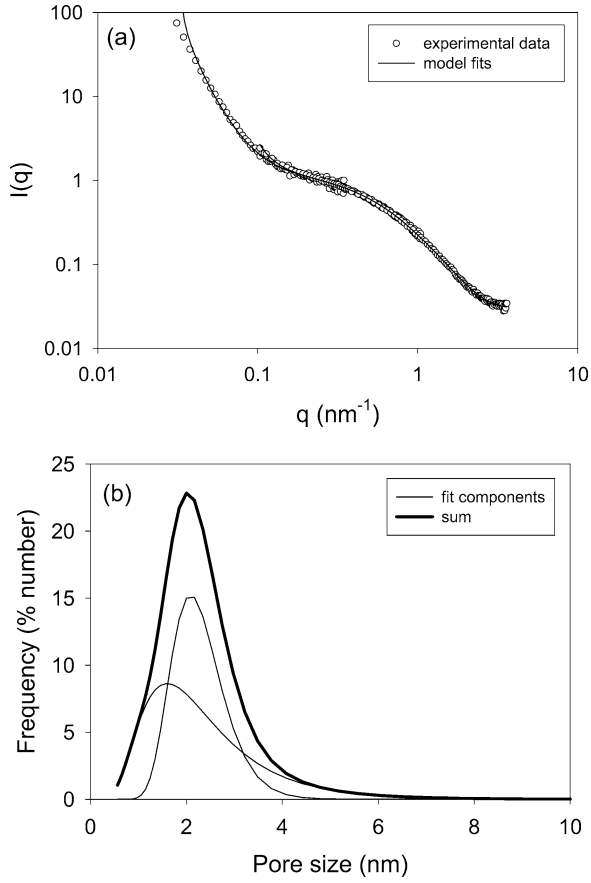

Fig. 4. Small-angle neutron scattering data for dense HFO aggregates in D_2O: (a) The experimental scattering intensity $I(q)$ as a function of scattering vector q is obtained with three different instrumental settings. The curve is well modeled by fitting two lognormal distribution curves. (b) Number frequency distribution of pore sizes as determined from the fitting of the experimental scattering data.

This weaker decay reflects a broad pore size distribution. With our fitting procedure for the analysis of the neutron scattering data, this distribution was best fitted by a combination of two lognormal size distributions. The scattering data are in quantitative agreement with a broad and unimodal pore size distribution with a maximum at 2.0 nm (Fig. 4b). No pores are detected above 15 nm. The porosity of the aggregates is thus exclusively composed of micro- and small mesopores.

While SANS provides information about the structure of the wet aggregates, N_2 gas adsorption can probe the surface area and the pore sizes of dried materials. The adsorption of water vapor also makes it possible to characterize the dry surface and the structure of the aggregate, but additionally gives insight into the wetting behavior of the material. The N_2 gas adsorption isotherm obtained after the outgassing of an HFO aggregate sample at $30\,^{\circ}\mathrm{C}$ is presented in Fig. 5a. The general shape of the isotherm suggests the presence of pores with diameters in the upper range of the classical micropore domain, around 1 to 2 nm [39]. This interpretation is confirmed by the moderate value of the C constant ($C = 126$) obtained with the BET equation fit (Table 1). If

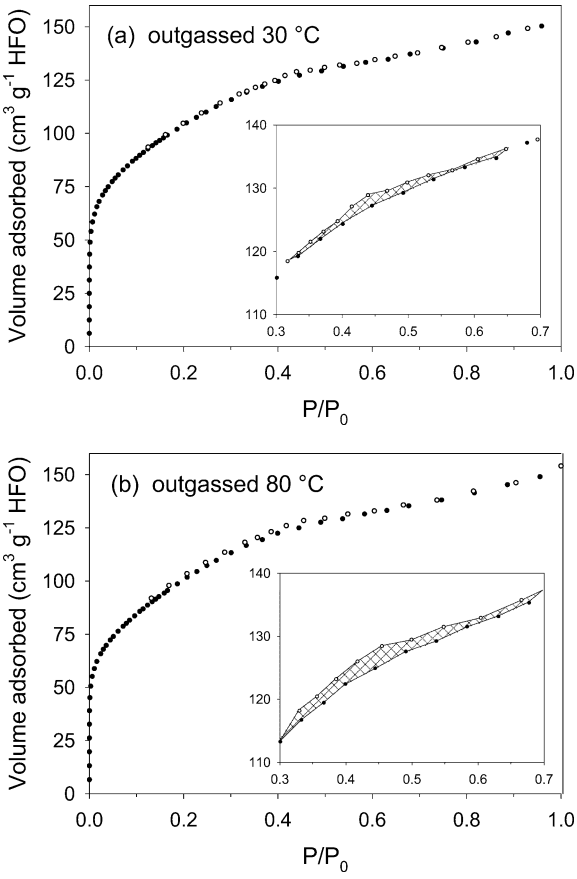

Fig. 5. N_2 gas adsorption (•) and desorption (○) isotherms for dense HFO aggregates formed by freezing a dialyzed HFO suspension at −25 °C: (a) HFO sample outgassed at 30 °C, (b) HFO sample outgassed at 80 °C. The enlargements show the small hysteresis effects.

smaller micropores were present, this value would be much higher, as is observed, for instance, for pillared clays or activated carbon [40,41].

In addition to micropores, small mesopores also appear to be present, as revealed by a tiny adsorption–desorption hysteresis for $0.35 < P/P_0 < 0.60$ (Fig. 5a, inset). Consequently, the nitrogen adsorption isotherm obtained for this sample reveals a continuous distribution of pore sizes in the range 1–5 nm. The external surface area is low, as indicated by the nearly flat profile of the isotherm for $P/P_0 \geqslant 0.60$.

After the outgassing of the HFO aggregates at higher temperatures, small changes in the N_2 gas adsorption isotherms were observed. The BET calculations resulted in a slightly smaller surface area and a lower C constant (Table 1). In contrast, the adsorption–desorption hysteresis was slightly larger and extended toward higher values of P/P_0 (Fig. 5b, inset). This shows that higher outgassing temperatures provoke a small shift of the pore size distribution toward slightly larger pores, resulting in an increase of the amount of mesopores at the expense of some micropores, and a decrease in specific surface area. These changes are related to the removal of surface hydroxyl groups and possibly some entrainment of structural hydroxyls [25]. Because the extent of

Table 1
Total specific surface area, total volume of gas adsorbed (V_m), and C constants obtained by the BET equation fit for N_2 gas adsorption isotherms of dense HFO aggregates outgassed at 30, 50, or 80 °C and for water vapor adsorption isotherms for aggregates outgassed at 30 °C

	Outgassing temperature		
	30 °C	50 °C	80 °C
BET analysis (N_2 gas)			
V_m ($cm^3\,g^{-1}$)	86.7	85.5	83.5
C constant	126.5	115.1	97.9
Specific surface area ($m^2\,g^{-1}$)	378.6	373.5	364.9
t-plot analysis (N_2 gas)			
Specific surface area ($m^2\,g^{-1}$)	366.5	366.4	352.4
External surface area ($m^2\,g^{-1}$)	15.6	15.5	16.9
		30 °C	
BET analysis (water vapor)			
V_m ($cm^3\,g^{-1}$)		277.5	
C constant		26.1	
Surface area for H_2O ($Å^2$)	10.6		14.8
Specific surface ($m^2\,g^{-1}$)	320.1		455.4

In the case of water, results are shown for two possible adsorption surface areas of the water molecule. t-plot analyses, performed for the N_2 gas adsorption data, determined the total and the external specific surface areas.

these changes cannot be quantified precisely, the most conservative isotherm, obtained after outgassing at 30 °C, will serve as the data basis for all derived calculations. At relative pressures above 0.7, the N_2 gas adsorption isotherms obtained after outgassing at 30, 50, or 80 °C were nearly identical, indicating similar external surface areas.

The t-plot analysis of the N_2 gas adsorption data confirmed the tendencies derived from the study of the raw isotherms. At all three outgassing temperatures, the shape of the t-plot is typical of a porous solid with a continuous pore distribution in the transition range between micropores and mesopores (Fig. 6). The straight line going through the origin extends to t-values corresponding to relative pressures around 0.30. The external surface area, similar at the three temperatures, lies between 15 and 17 $m^2\,g^{-1}$ (Table 1). The tiny shift in pore sizes toward higher values between samples outgassed at 30 and 80 °C is also noted on the t-plot: the point at which the straight line going through the origin deviates from the experimental data (indicated by an arrow in Fig. 6) moves from $t = 4.88$ for outgassing at 30 °C to 5.27 for outgassing at 80 °C. The t-plot allows a derivation of the total micropore volume. In the present case, the line fitting the plateau at the end of the curve (Fig. 6) and intersecting the y-axis gives an estimate of the micro- and small mesopore volume. The gas volume adsorbed (132 $cm^3\,g^{-1}$ HFO) transforms to 46.5% porosity. For microporosity only, the best possible estimate is derived from a line tangent to the base of the t-plot curvature. The gas volume adsorbed is 60 $cm^3\,g^{-1}$ HFO or, expressed in pore volume, 0.1 $cm^3\,g^{-1}$.

The BJH analysis of the N_2 gas desorption data gives additional information on the porosity in the pore size range from 2 to 95 nm. The size distribution of the mesopores is

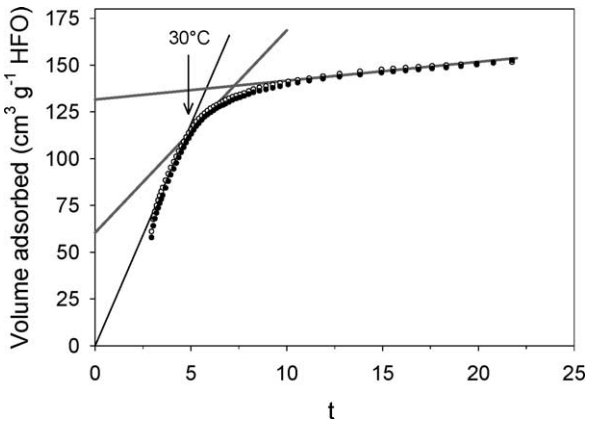

Fig. 6. t-plot analysis of N_2 gas adsorption isotherms for dense HFO aggregates formed by freezing a dialyzed HFO suspension at −25 °C. The samples were outgassed at 30 °C (○) or 80 °C (●), respectively. The arrow indicates the point of deviation of the 30 °C data (○) from a linear fit. The line fitting the plateau intersects the y-axis at 132 cm^3 g^{-1} HFO. This amount represents the total micropore and small mesopore volume. The line tangent to the t-plot curvature intersects the y-axis at 60 cm^3 g^{-1} HFO, giving an estimate of the micropore volume only.

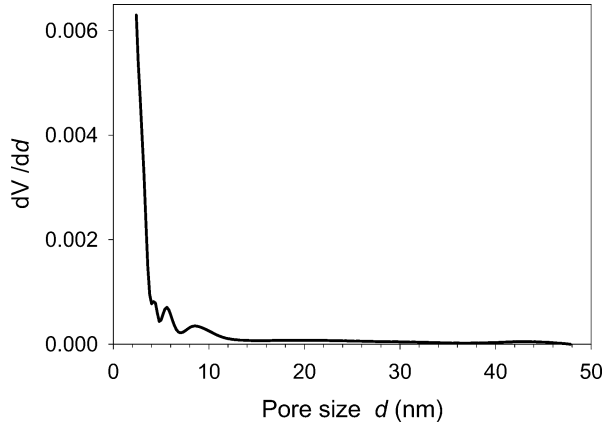

Fig. 7. Volume distribution of mesopores of dense HFO aggregates formed by freezing a dialyzed HFO suspension at −25 °C. The curve was derived from the BJH analysis of N_2 gas desorption data of the sample outgassed at 30 °C.

best viewed by the derivative of the volumetric pore size distribution (Fig. 7). The curve increases drastically below 5 nm, again confirming that porosity is essentially located in the micropore-to-small-mesopore size range. Total pore volume in the range 2–95 nm amounts to 0.16 cm^3 g^{-1} HFO. Combined with the micropore volume inferred from the t-plot, a porosity of 50% is obtained. This compares satisfactorily with the total micro- and mesoporosity obtained by t-plot analysis, so that a good estimate of the porosity of dry aggregates is 46–50%. This value does not include large pores such as desiccation cracks.

The water vapor adsorption isotherm obtained after outgassing at 10^{-9} bar and 30 °C for 18 h is presented in Fig. 8. Under these gentle dehydration conditions, surface hydroxyls (chemisorbed water) are retained at the surface to a great extent [42]. Therefore the present water vapor adsorption isotherm is mainly due to physisorption of water molecules and can be compared with the N_2 gas adsorption isotherm of the same sample (Fig. 8). The quantity of water adsorbed increased nearly linearly for P/P_0 between 0.10 and 0.70, thus revealing a continuous filling of pores with increasing sizes. For high relative water vapor pressures, the adsorbed amounts do not increase any further, indicating that the external surface area of the HFO aggregates is almost negligible. When expressed in liquid volume, the adsorbed quantities are similar for nitrogen and water at high relative pressure, suggesting that water adsorption is not associated to textural changes. The BET surface area for water is equal to 320 m^2 g^{-1}, assuming a cross-sectional area of 10.6 Å^2 [39], and to 455 m^2 g^{-1}, assuming a cross-sectional area of 14.8 Å^2 [43].

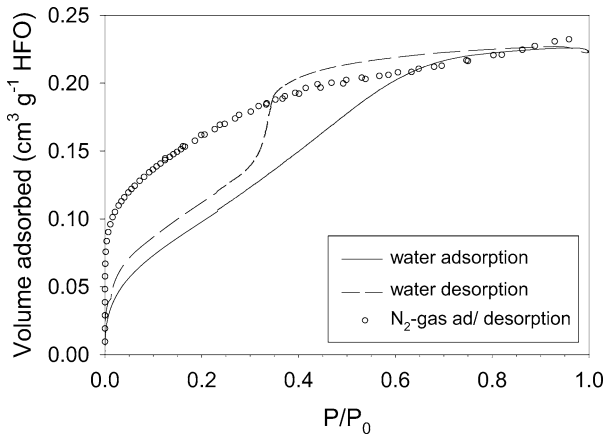

Fig. 8. Water vapor and N_2 gas adsorption and desorption isotherms obtained for dense HFO aggregates outgassed at 30 °C. For better comparison, the equivalent liquid volume of sorbed gas is plotted in both cases.

The C constant determined by fitting the BET equation to the water vapor adsorption isotherms was equal to 26.1. As the solid is strongly porous and thus is favoring sorbate condensation, a cross-sectional area of 10.6 Å^2, corresponding to hexagonal closest packing as in liquid water, seems more appropriate. Under this assumption, the water BET surface area would be lower than the value determined by N_2 gas adsorption (Table 1), which could be due to the smaller size of the water molecule. Indeed, some pores that are micropores for N_2 may be mesopores for water. This interpretation is supported by the shape of the desorption branch, which presents a much larger hysteresis than in the case of nitrogen.

4. Discussion

Freezing a dialyzed HFO suspension at −25 and −196 °C was shown to result in the formation of dense HFO aggregates with average diameters of 235 µm (Fig. 3a) and 20 µm, respectively (Fig. 3b). This confirms experimental results of Zolotavin et al. [8], who found the largest aggregates at freezing temperatures of −1 °C and a progres-

sive decrease of sizes with lower freezing temperatures. The process responsible for the formation of dense HFO aggregates is related to cryosuction during the crystallization of water at temperatures below the freezing point [13]. Shock freezing without crystallization of water only occurs when a small volume (few µl) of water is plunged into liquid nitrogen (−196 °C) or liquid helium (−270 °C). When a larger volume of water is frozen, as was the case in this study (500-ml samples), the heat conduction of water and ice limits instantaneous freezing and therefore water can form large ice crystals. Ice formation starts at the interface with the cooling medium (e.g., air or liquid N_2) and progresses inward. In a slowly freezing suspension, particles are excluded from the forming ice and tend to accumulate in the remaining liquid water near the progressing freezing front. When a sufficient number of particles obstruct this surface, free water is withdrawn from the intraparticle space by diffusion toward the ice front (cryosuction). Thereby, the HFO crystallites are pushed together to form dense aggregates. With increasing freezing rate, the progressing ice front changes from smooth to dendritic [17], thereby entrapping HFO aggregates between prograding ice needles, ultimately leading to the formation of smaller HFO aggregates.

Addition of electrolytes to the HFO suspension before freezing resulted in the formation of smaller aggregates. The freezing temperature and the eutectic temperature of the given electrolyte both influence the aggregate formation. If the freezing temperature is above the eutecticum, the electrolyte solution will freeze only partially [44]. The suspended particles accumulated in the remaining solution will not be compressed [10]. In our experiments, the freezing temperature was below the eutecticum. In this case, the solution freezes out completely once the eutectic temperature is reached. However, as the electrolyte concentration increases, the viscosity of the solution also increases, which has an effect similar to that of increasing the freezing rate [45,46]: Engulfment of the particles in the growing ice crystals is facilitated. The higher the electrolyte concentration was initially, the lower the "critical freezing rate" [45] and the smaller will be the compacted HFO entities.

The particle/water interface of oxides and hydroxides is characterized by a layer of hydration water consisting of a layer of chemically bound and several layers of oriented water molecules. The full extent of the hydration layer is not precisely defined but lies in the nanometer range. Pashley and Israelachvili [47,48], experimenting with mica surfaces, showed that hydration forces occur at distances below approximately 1 nm. Using microcalorimetry of immersion, Fripiat and collaborators [49] determined a maximum of three statistical H_2O layers on clay surfaces, that is, a hydration layer of thickness approximately 0.9 nm. It is most likely that the compression during freezing does not overcome these forces and that one or more H_2O layers are therefore conserved in the dense HFO aggregates [8]. The fact that compression is not reversed upon thawing of the HFO aggregates indicates that freezing induces coagulation, with HFO crystallites moving into a primary energy minimum. They can, however, be redispersed by applying high shear forces, e.g., by ultrasonic treatment, which suggests that only electrostatic bonding occurs during cryocoagulation. In the 1970s, the DLVO theory [50,51] of colloidal stability was adapted to include particles with a hydration layer such as oxides and hydroxides [52]. The surface electric potential responsible for the electrostatic repulsion energy was replaced by the electric potential at the Stern plane. The Stern correction implies that the primary energy minimum is displaced from the surface to the Stern plane, some 0.3 to 1 nm away [53,54]. Although the hydration layer and the Stern layer are not identical, their outer boundaries are related. These theoretical considerations suggest that freezing leads to coagulation of the HFO crystallites in the primary energy minimum situated at the Stern plane. Compressed crystallites are therefore expected to lie two Stern layers or 0.6 to 2 nm apart.

The dense HFO aggregates formed by freezing and thawing were shown to have a porosity of $73 \pm 2\%$, with most pores in the size range 1–5 nm. To help to appreciate the meaning of this porosity, let us consider a cubic close packing of spheres with diameter 2 nm, which corresponds to the unit crystallite size of the HFO determined by TEM. When the unit particles are in direct contact with one another, the diameter of voids between the spheres is 0.83 nm and the porosity is 26%. This geometric arrangement is the tightest possible packing of spheres. Now envision that the unit particles maintain their hydration layer during aggregate formation. Keeping the assumed cubic close packed arrangement, the resulting porosity and pore size will be significantly higher, depending on the thickness of the hydration layer. For example, a minimum contact distance of 0.9 nm would produce a total porosity of 75% and a maximum diameter of interstitial pores of 2.1 nm. Although the structure assumption is hypothetical, it nicely illustrates that the measured porosity of the dense HFO aggregates corresponds to a high degree of compaction. It is also interesting to note that the calculated minimum contact distance for 75% porosity corresponds to three hydration layers of water, which is in good agreement with the theoretical DLVO considerations discussed earlier.

The average pore size of the HFO aggregates determined by SANS was 2.0 nm, which would confirm the image of a cubic close packing of hydrated 2-nm spheres. At first sight, this coincidence may support the idea of a regular geometric structure of the aggregates. However, the experimental evidence from SANS and gas adsorption isotherms indicates a broad distribution of pore sizes in the range 1 to 5 nm. This may partly be explained by size heterogeneity of unit particles. More probably, it reflects a cluster–cluster mode of formation of dense HFO aggregates. Nonetheless, the peak at 2.0 nm strongly suggests that the distance of closest approach between the crystallites is about three H_2O layers, as calculated above. In such pore systems, fractal arrangements are frequently observed. In a SANS experiment, pore frac-

tality would lead to a power-law-like q-dependence $I(q) \sim q^{-d_F}$, where d_F is the fractal dimension of the pore network, for q-values in the range 1/(HFO particle size) $\ll q \ll$ pore size. Our data do not extend to low enough q-values to reach the asymptotic region, where a fractal dimension could be unambiguously determined. However, some data are available from the literature. For fresh HFO aggregates, the fractal dimension at low ionic strength strongly depends on the mixing rates of the suspension. Lo and Waite [37], examining the small-angle light scattering behavior of HFO, estimated D values from 1.5 to a maximum of 2.6, depending on the rate and duration of mixing. Weidler and Stanjek [55] determined a surface fractal dimension of 2.7–2.8 for a freeze-dried two-line ferrihydrite, based on gas adsorption isotherms. For the dense HFO aggregates in the present study, we can expect a dimension between 2.5 and 2.8.

The porosity of dried HFO aggregates was only $48 \pm 5\%$, which suggests a reduction in pore space upon dehydration by about 25%. This reduction in porosity is accompanied by a change in the pore size distribution. In Fig. 9 we compare the cumulative pore size distributions determined by SANS for wet aggregates and by the t-plot and BJH analysis of N_2 gas adsorption isotherms for the dry HFO aggregates. The curve for dry aggregates is shifted towards smaller pore diameters due to an increase of pores smaller 3 nm. This effect must be related to evaporation of hydration water during outgassing of HFO aggregates and a consequent shrinkage of the pore sizes. For the wet aggregates, practically no pores are detected above 15 nm, whereas 5% of the pores in the dry aggregates are larger than 15 nm. This suggests a widening of larger mesopores upon dehydration and evacuation in a vacuum chamber.

Dehydration of the dense HFO aggregates may also have an influence on the specific surface area. The theoretical surface area of HFO crystallites with an average size of 2 nm and a density of 4 $g\,cm^{-3}$ is 750 $m^2\,g^{-1}$. A frequently proposed value for HFO is 600 $m^2\,g^{-2}$ [1,56–58]. However,

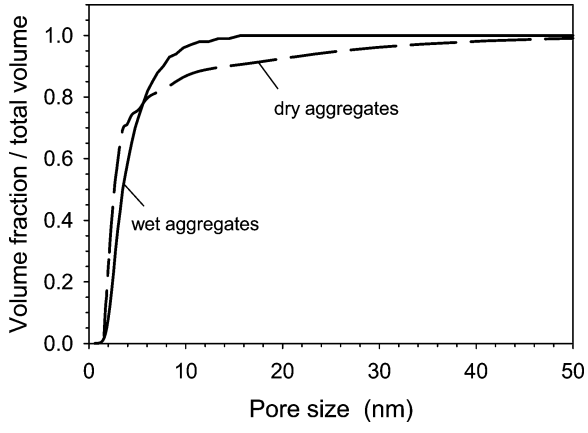

Fig. 9. Cumulative volume distribution of pore sizes in wet HFO aggregates as determined by SANS and in dry HFO aggregates as determined by N_2 gas adsorption. The curve for dry aggregates is obtained from the combined results of BJH and t-plot analyses of the sample outgassed at 30 °C.

the results obtained by gas adsorption experiments (Table 1) are significantly lower. Several aspects may be considered to explain this difference. During precipitation of HFO, intercrystallite bonds may form that will reduce the theoretical surface area. Additionally, the HFO we used in this study was aged over 15 days during dialysis. It has been noted [4,5] that the sorption capacity of HFO decreases significantly during the first hours to days of aging. This reduction is related to restructuring of the HFO mineral and is certainly accompanied by a reduction of the surface area. The specific surface areas obtained by gas adsorption represent accessible surfaces of the dry aggregates. Since during degassing hydration water is removed, it is probable that the primary energy minimum of coagulation is displaced toward the crystallite surface and that the attractive forces increase. Thereby new chemical bonds may be formed between neighboring crystallites (hydrogen bonds, oxolation), leading to a reduction in accessible surface area. This hypothesis is supported by the observation that water vapor adsorption was not able to reverse the aggregate structure from dry to wet.

5. Conclusions

The cryoaggregation process induced by freezing HFO suspensions at −25 °C and subsequent thawing at room temperature leads to the formation of dense HFO aggregates with an internal porosity of 73%. About 70% of the pore volume is in mesopores 2 to 5 nm in diameter, and 8% in micropores 1 to 2 nm in diameter; the remaining 22% is located in pores between 5 and 15 nm. The pore size distribution was shown to be unimodal, with an average pore diameter of 2.0 nm. Geometric considerations suggest that the approximately 2-nm large unit crystallites of HFO retain a hydration layer of water during the freezing process and that the primary energy minimum of coagulation may be situated one to two water layers away from the crystallite surface. This would imply that the pores formed during freezing remain continuously connected and that no surface area is consumed by formation of dense HFO aggregates at −25 °C. As a consequence, it seems likely that the chemical surface reactivity of these dense HFO aggregates is comparable to that of the fresh HFO before freezing. However, the kinetics of cation and anion adsorption onto the dense HFO aggregates might be influenced by the specific distribution of micro- and mesopores, which will limit ion diffusion. The observations made in this study do suggest that slow freezing mainly generates pores in the region large micropores–small mesopores.

The pore structure changes significantly upon dehydration of the HFO dense aggregates. The fraction of micropores increases to 25% of the total pore volume at the expense of small mesopores. This shift indicates that the unit crystallites are pushed together during drying. The aggregate shrinkage may be irreversible as rehydration of the surfaces by water vapor does not have any swelling effect on the

pores. We postulate that drying could lead to the formation of new chemical bonds between HFO crystallites. The specific surface area of 320 to 380 $m^2\,g^{-1}$ derived from gas adsorption isotherms may therefore be significantly smaller than the surface area of the wet aggregates. This would imply that the chemical reactivity of dried HFO aggregates is lower.

Acknowledgments

Martin Müller (ETH Zurich) is gratefully acknowledged for his invaluable technical assistance in electron microscopy and stimulating discussions. We thank Frédéric Villéras (LEM Nancy) for assisting in the treatment and interpretation of gas adsorption data, Michael Plötze (ETH Zurich) for X-ray diffraction analysis, and Kurt Barmettler (ETH Zurich) for his technical support in the soil chemistry laboratory.

References

[1] D.A. Dzombak, F.F. Morel, Surface Complexation Modeling. Hydrous Ferric Oxide, Wiley, New York, 1990.
[2] R.M. Cornell, U. Schwertmann, The Iron Oxides, VCH Verlagsgesellschaft mbH, Weinheim, 1996.
[3] C.P. Lienemann, M. Monnerat, J. Dominik, D. Perret, Aquat. Sci. 61 (1999) 133.
[4] C.C. Fuller, J.A. Davis, G.A. Waychunas, Geochim. Cosmochim. Acta 57 (1993) 2271.
[5] L. Lijklema, Environ. Sci. Technol. 14 (1980) 537.
[6] P.E. Kneebone, A. O'Day, N. Jones, J.G. Hering, Environ. Sci. Technol. 36 (2002) 381.
[7] N.N. Lyubavin, Zh. Russ. Fiz.-Khim. O. 21 (1889) 397.
[8] V.L. Zolotavin, V.V. Vol'khin, V.V. Rezvushkin, Colloid J. 22 (1960) 305.
[9] C.J. Martel, Water Sci. Technol. 30 (1994) 177.
[10] V.V. Vol'khin, V.L. Zolotavin, Colloid J. 23 (1961) 134.
[11] V.V. Vol'khin, V.L. Zolotavin, S.A. Tipikin, Colloid J. 23 (1961) 404.
[12] V.L. Zolotavin, V.V. Vol'khin, Colloid J. 23 (1961) 276.
[13] V.V. Vol'khin, E.I. Ponomarev, Colloid J. 27 (1965) 14.
[14] A.A. Van der Giessen, J. Inorg. Nucl. Chem. 28 (1966) 2155.
[15] V.S. Pakholkov, V.M. Bochkarev, Radiokhimiya 22 (1980) 25.
[16] D. Nickols, G.C. Moerschell, M.V. Broder, Water Sci. Technol. 31 (1995) 239.
[17] P.J. Parker, A.G. Collins, J.P. Dempsey, J. Environ. Eng. ASCE 124 (1998) 249.
[18] W. Driehaus, M. Jekel, U. Hildebrandt, J. Water SRT-Aqua 47 (1998) 30.
[19] G.P. Brovka, I.V. Dedyulya, Colloid J. 58 (1996) 586.
[20] M. Hohmann, Cold Regions Sci. Technol. 25 (1997) 101.
[21] L. Axe, P.R. Anderson, J. Colloid Interface Sci. 175 (1995) 157.
[22] N.J. Barrow, J. Soil Sci. 34 (1983) 733.
[23] A.C. Scheinost, S. Abend, K.I. Pandya, D.L. Sparks, Environ. Sci. Technol. 33 (2001) 1090.
[24] U. Schwertmann, R.M. Cornell, Iron Oxides in the Laboratory, VCH Verlagsgesellschaft mbH, Weinheim, 1991.
[25] H. Stanjek, P.G. Weidler, Clay Miner. 27 (1992) 397.
[26] J.E. Poirier, M. François, J.M. Cases, J. Rouquerol, in: A.I. Liapis (Ed.), Proceedings of the Second Engineering Foundation Conference on Fundamentals of Adsorption, AIChE Pub., New York, 1987, p. 473.
[27] S. Brunauer, P.H. Emmett, E. Teller, J. Am. Chem. Soc. 60 (1938) 309.
[28] J.H. De Boer, B.G. Lippens, J.C.P. Broekhoff, A. Van den Heuvel, T.J. Osinga, J. Colloid Interface Sci. 21 (1966) 405.
[29] J. Hagymassy, S. Brunauer, R.S. Mikhail, J. Colloid Interface Sci. 29 (1969).
[30] E.P. Barrett, L.G. Joyner, P.P. Halenda, J. Am. Chem. Soc. 73 (1951) 373.
[31] C. Pierce, J Phys. Chem. 57 (1953) 149.
[32] J.S. Pedersen, D. Posselt, K. Mortensen, J. Appl. Crystallogr. 23 (1990) 321.
[33] J.P. Barker, J.S. Pedersen, J. Appl. Crystallogr. 28 (1995) 105.
[34] P.R. Bevington, Data Reduction and Error Analysis for Physical Sciences, McGraw–Hill, New York, 1969.
[35] M.I. Zapata, J.R. Feldkamp, G.E. Peck, J.L. White, S.L. Hem, J. Pharm. Sci. 73 (1984) 3.
[36] D.E. Janney, J.M. Cowley, P.R. Buseck, Clays Clay Miner. 48 (2000) 111.
[37] B. Lo, T.D. Waite, J. Colloid Interface Sci. 222 (2000) 83.
[38] K.M. Towe, W.F. Bradley, J. Colloid Interface Sci. 24 (1967) 384.
[39] S.J. Gregg, K.S.W. Sing, Adsorption, Surface Area and Porosity, Academic Press, London, 1982.
[40] J.M. Cases, Y. Grillet, M. François, L. Michot, F. Villiéras, J. Yvon, Clays Clay Miner. 39 (1991) 191.
[41] L.J. Michot, F. Didier, F. Villiéras, J.M. Cases, Y. Grillet, A. Bouchelaghem, in: B. McEnaney, T.J. Mays, J. Rouquerol, F. Rodriguez-Reinoso, K.S.W. Sing, K.K. Unger (Eds.), Characterization of Porous Solids IV, Royal Society of Chemistry, London, 1997, p. 374.
[42] T. Morimoto, M. Nagao, F. Tokuda, J. Phys. Chem. 73 (1969) 243.
[43] W.D. Harkins, G. Jura, J. Am. Chem. Soc. 66 (1944) 1362.
[44] C.W. Correns, Einführung in die Mineralogie, Springer-Verlag, Berlin, 1968.
[45] W.R. Wilcox, J. Colloid Interface Sci. 77 (1980) 213.
[46] G. Gupta, R.F. Rice, W.R. Wilcox, J. Colloid Interface Sci. 82 (1981) 458.
[47] R.M. Pashley, J. Colloid Interface Sci. 80 (1981) 153.
[48] R.M. Pashley, J.N. Israelachvili, J. Colloid Interface Sci. 101 (1984) 511.
[49] J.J. Fripiat, J.M. Cases, M. François, M. Letellier, J.F. Delon, J. Rouquerol, in: J. Rouquerol, K.S.W. Sing (Eds.), Adsorption at the Gas–Solid and Liquid–Solid Interface, Elsevier, Amsterdam, 1982, p. 449.
[50] B.V. Derjaguin, L.D. Landau, Acta Physicochim. 14 (1941) 633.
[51] E.J.W. Verwey, J.T.G. Overbeek, Theory of the Stability of Lyophobic Colloids, Elsevier, Amsterdam, 1948.
[52] J. Lyklema, in: K.J. Ives (Ed.), The Scientific Basis of Flocculation, Sijthoff & Noordhoff, Alphen aan den Rijn, 1978, p. 3.
[53] T. Hiemstra, W.H. Van Riemsdijk, Colloids Surf. 59 (1991) 7.
[54] D.A. Sverjensky, Geochim. Cosmochim. Acta 65 (2001) 3643.
[55] P.G. Weidler, H. Stanjek, Clay Miner. 33 (1998) 277.
[56] J.A. Davis, J.O. Leckie, J. Colloid Interface Sci. 67 (1978) 90.
[57] S.N. Luoma, J.A. Davis, Mar. Chem. 12 (1983) 159.
[58] E.E. Roden, J.M. Zachara, Environ. Sci. Technol. 30 (1996) 1618.